Selective changes of resting-state networks in individuals at risk for Alzheimer's disease

Christian Sorg*†, Valentin Riedl‡§, Mark Mühlau‡, Vince D. Calhoun¶‖, Tom Eichele**, Leonhard Läer††, Alexander Drzezga‡‡, Hans Förstl*, Alexander Kurz*, Claus Zimmer††, and Afra M. Wohlschläger‡†††‡‡

Departments of *Psychiatry, ‡Neurology, ††Neuroradiology, and ‡‡Nuclear Medicine, Klinikum Rechts der Isar, Technische Universität München, Ismaningerstrasse 22, 81675 Munich, Germany; ¶MIND Institute, 1101 Yale Boulevard, Albuquerque, NM 87131; ‖Department of Electrical and Computer Engineering, University of New Mexico, Albuquerque, NM 87131; **Cognitive Neuroscience Group, Faculty of Psychology, University of Bergen, Jonas Lies Vei 91, 5011 Bergen, Norway; and §Munich Center for Neurosciences, Brain and Mind, Ludwig-Maximilians Universität; Grosshadernerstrasse 2, 82152 Martinsried, Germany

Edited by Leslie G. Ungerleider, National Institutes of Health, Bethesda, MD, and approved September 25, 2007 (received for review September 17, 2007)

Alzheimer's disease (AD) is a neurodegenerative disorder that prominently affects cerebral connectivity. Assessing the functional connectivity at rest, recent functional MRI (fMRI) studies reported on the existence of resting-state networks (RSNs). RSNs are characterized by spatially coherent, spontaneous fluctuations in the blood oxygen level-dependent signal and are made up of regional patterns commonly involved in functions such as sensory, attention, or default mode processing. In AD, the default mode network (DMN) is affected by reduced functional connectivity and atrophy. In this work, we analyzed functional and structural MRI data from healthy elderly ($n = 16$) and patients with amnestic mild cognitive impairment (aMCI) ($n = 24$), a syndrome of high risk for developing AD. Two questions were addressed: (*i*) Are any RSNs altered in aMCI? (*ii*) Do changes in functional connectivity relate to possible structural changes? Independent component analysis of resting-state fMRI data identified eight spatially consistent RSNs. Only selected areas of the DMN and the executive attention network demonstrated reduced network-related activity in the patient group. Voxel-based morphometry revealed atrophy in both medial temporal lobes (MTL) of the patients. The functional connectivity between both hippocampi in the MTLs and the posterior cingulate of the DMN was present in healthy controls but absent in patients. We conclude that in individuals at risk for AD, a specific subset of RSNs is altered, likely representing effects of ongoing early neurodegeneration. We interpret our finding as a proof of principle, demonstrating that functional brain disorders can be characterized by functional-disconnectivity profiles of RSNs.

default mode network | intrinsic brain activity | mild cognitive impairment

Alzheimer's disease (AD) is a neurodegenerative disorder clinically characterized by progressive dementia and neuropsychiatric symptoms (1). AD is neuropathologically defined by tau pathology and amyloid aggregations (2). Tau pathology starts in regions of the medial temporal lobe (MTL) and is well correlated with cell loss and atrophy; amyloid deposition primarily affects distributed neocortical regions but is not especially prominent in the MTL (2, 3). Atrophy of the MTL is correlated with the degree of dementia and also the extent of temporoparietal hypometabolism; both results are assumed to reflect changes in cerebral connectivity, especially between the MTL and the neocortex (3–5). In non-human primates, prominent structural connectivity between the MTL and neocortical regions as well as broad neocortical hypometabolism after ablation of parts of the MTL were demonstrated (6, 7). Evidence for disrupted structural and functional connectivity (FC) further suggests that AD includes a disconnection syndrome (5, 8–10).

Mild cognitive impairment (MCI) is a syndrome with cognitive decline greater than expected for an individual's age and educational level but not interfering notably with activities of daily living; prevalence of MCI is ≈15% in adults older than 65 years; more than half of patients with MCI progress to dementia within 5 years; the amnestic subtype of MCI has a high risk of progression to AD constituting a prodromal stage of AD (1, 11, 12). Previous results of task-related functional MRI (fMRI) in patients with MCI (13, 14) indicate that FC seems to be already impaired in prodromal stages of AD (15). Reduced white matter volumes of the MTL in amnestic MCI (aMCI) point at changed MTL–neocortex connectivity (16). Very recent fMRI studies in AD reported on FC changes especially during rest (5, 9, 17). Together, these findings suggest that the functional integration of brain areas in the cerebral resting state in individuals at risk for AD is disturbed and that functional changes are related to MTL atrophy.

The study of intrinsic brain activity may be central for understanding the physiology of functional brain disorders (5, 18–20). Functional brain disorders such as AD, schizophrenia, or autism are characterized by structural alterations that are subtle or have an uncertain relationship to clinical symptoms (21). Such structural lesions might be functionally related to alterations of intrinsic brain activity that are reflected by changes of connectivity (18, 19). Here, the study of spontaneous coherent fluctuations of the blood oxygen level-dependent (BOLD) signal at rest by fMRI is of special interest. Synchronized BOLD fluctuations overlap with brain systems that are involved in functions such as motor, sensory, language, attention, or default mode processing (22–28). Evidence for the neuronal nature of so-called resting state networks (RSNs) comes from studies that employ simultaneous fMRI and electroencephalograms (EEGs) (29, 30), from the observation of altered connectivity caused by neurological diseases (5), and from the existence of homologous RSNs in non-human primates that overlap with neuroanatomically defined systems (31).

Regions including the posterior cingulate, inferior parietal, and medial prefrontal cortex, constitute a RSN called default mode network (DMN) (32, 33). The areas of the DMN show consistently greater BOLD activity during rest than during any attention-demanding task, a phenomenon called deactivation; the same regions are prominently involved in episodic memory processes together with the MTL; their spontaneous fluctuations at rest are anticorrelated to the spontaneous fluctuations of a widely distributed neocortical system that largely overlaps with attention-related RSNs (5, 22, 27, 28, 32, 34–36). In AD, parietal

Author contributions: C.S. and V.R. contributed equally to this work; C.S., A.D., H.F., A.K., and A.M.W. designed research; C.S., L.L., H.F., A.K., C.Z., and A.M.W. performed research; V.D.C. and T.E. contributed new reagents/analytic tools; C.S., V.R., M.M., and A.M.W. analyzed data; and C.S., V.R., and A.M.W. wrote the paper.

The authors declare no conflict of interest.

This article is a PNAS Direct Submission.

Freely available online through the PNAS open access option.

†To whom correspondence should be addressed. E-mail: c.sorg@lrz.tum.de.

This article contains supporting information online at www.pnas.org/cgi/content/full/0708803104/DC1.

Table 1. Subject demographic information

Parameter	NC	MCI
n	16	24
Age, years	68.1 ± 3.8	69.3 ± 8.1
Sex, male/female	10/6	13/11
Education, </>12 years	10/6	14/10
CDR, sum of boxes	0 ± 0	2.2 ± 0.9*
MMSE	29.6 ± 0.5	27.7 ± 1.1*
CERAD (delayed recall)	7.4 ± 1.3	4.3 ± 2.1*

Data are presented as mean ± SD. NC, normal control; CDR, Clinical Dementia Rating scale; MMSE, Mini-Mental State Exam; CERAD, Consortium to Establish a Registry for Alzheimer's Disease. *, $P < 0.05$ difference between groups.

regions of the DMN demonstrate altered functional connectivity at rest within the DMN itself, to the MTL, and to neocortical areas that are involved in attention processes (5, 9, 17). Accounting for these findings, the hypothesis suggested above of altered FC at rest in individuals at high risk for AD can be specified in terms of RSNs with a focus on FC changes in the DMN and attention-related RSNs. In general, the finding of RSNs allows for a broadened perspective on functional brain disorders in the field of neuroimaging: the brain shows rich intrinsic dynamics in absence of tasks, with external stimuli more modulating than determining brain activity (19, 20, 27, 31, 37); the plurality of RSNs reflects this structured intrinsic activity, and selective changes of RSNs may characterize traits and states of functional brain disorders such as AD (18, 19, 21, 26).

Most previous studies investigating RSNs have used region-of-interest (ROI)-based correlation analyses (9, 17, 22–24). The signal time course of a selected ROI is correlated with remaining brain areas, resulting in a ROI specific correlation map. More recently, instead of defining *a priori* spatial hypotheses, a number of studies used model-free approaches involving independent component analysis (ICA) to describe RSNs in rest-fMRI data (5, 25, 26, 30). ICA allows for the extraction of distinct spatio-temporal patterns by identifying spatially independent and temporally synchronous brain regions (38).

In the present work, we combined ICA and ROI-based correlation methods to investigate RSNs in patients with aMCI. We focused on the following questions: (*i*) Are any RSNs changed in aMCI compared with healthy elderly? (*ii*) Are there any volumetric changes in the patient group pointing at possible ongoing neurodegeneration? (*iii*) How are potential functional and structural changes related with respect to their spatial extent?

We examined 24 patients and 16 healthy elderly (Table 1). Participants were instructed to close their eyes and relax during 4 min of fMRI scanning. Rest-fMRI data were analyzed by using a group ICA approach involving subject-wise concatenation of the individual fMRI data sets and subsequent back-projection into subject space (15, 39). Voxel-based morphometry (VBM) of additional structural MRI data and ROI-based correlation analyses of the rest-fMRI data were performed to analyze possible causes of altered functional connectivity.

Results

RSNs in Healthy Elderly and Patients with aMCI. The ICA was performed employing a group ICA model for fMRI data (GIFT).[§§] After the IC estimation on the subject-wise concatenated data, the toolbox performs the analysis in three stages: data reduction through principal component analysis (PCA), ICA decomposition of aggregate data, and subsequent back-reconstruction of individual subject maps and time courses (39, 40). Results of the separate analyses for each study group are depicted in Fig. 1 [see also supporting information (SI) Table 2]. Each group IC image contains a pair of two spatial IC patterns that are correlated (red) or anticorrelated (blue) with the time course of the component (data not shown). In the corresponding glass brain projection, the result of a one-sample *t* test for the back-reconstructed individual subject IC patterns across both groups is shown [$P < 0.05$ false discovery rate (FDR) corrected for multiple comparisons]. Eight IC patterns represented functionally relevant RSNs as described previously (26). Both IC patterns of Fig. 1e/E and f/F were pairwise anticorrelated within one IC. The first two IC patterns of Fig. 1 partly coincide with the visual cortex: a/A covers inferior parts of the occipital cortex such as the striate area [Brodmann area (BA) 17/18]; b/B shows lateral and dorsal parts of the occipital gyrus (BA 19). The transverse (BA 41) and superior temporal gyrus (BA 22/42) of the auditory cortex are depicted in Fig. 1c/C. Fig. 1d/D represents a right lateralized frontoparietal network comprising the supramarginal gyrus (BA 39/40), middle temporal gyrus (BA 21), and middle frontal gyrus (BA 8) on the right side as well as bilateral frontal areas covering middle and inferior frontal gyrus (BA 8/9/46). This network is consistent with a ventral/reorienting attention network (34).

In Fig. 1e/E the upper IC pattern covers medial and lateral parts of the superior parietal lobe as well as the precuneus (BA 7). This network is constituted by areas well known to be active during spatial attention (41). The anticorrelated network of Fig. 1e/E (blue) includes a number of areas relevant for sensorimotor coordination in pre- and postcentral gyri (BA 3/4), the caudal zone of the cingulate motor cortex (BA 24), and parts of the superior frontal gyrus (BA 8) (41). The upper IC pattern of Fig. 1f/F includes medial prefrontal areas (BA 9/10/11), anterior (BA 12/32), and posterior cingulate cortex (PCC) (BA 23/31), the inferior temporal gyrus (BA 21), and bilateral supramarginal gyrus (BA 39) in the parietal lobe. This pattern corresponds to the DMN (26, 32, 42). Involvement of the hippocampus (HC), as seen by Greicius *et al.* (5), was not observed here. The anticorrelated network of Fig. 1f/F covers the superior parietal lobe (BA 7/40), V5/MT, and inferior temporal gyrus (BA 37), as well as parts of the inferior frontal gyrus mainly on the right side. These areas comprise a dorsal/executive attention network (34).

Altered RSNs in Patients with aMCI. The second analysis aimed at between-group differences in corresponding RSNs. We performed a two-sample *t* test on each of the eight RSNs contrasting the individual, back-reconstructed IC patterns of both groups. The only contrasts revealing any group difference concerned both IC patterns of Fig. 1f/F and are shown in Fig. 2 ($P < 0.05$, FDR corrected). None of the two-sample *t* tests on the five remaining components revealed significant group difference at $P < 0.001$, uncorrected for multiple comparisons (cluster extent threshold, 15 voxels). The following areas of the DMN associated IC pattern demonstrated reduced component time course-related activity in the patient group (see also SI Table 3): left PCC (BA 31), right medial prefrontal cortex (BA 10), and two small clusters in parietal cortex bilaterally (BA 39). Accordingly, we found reduced activity in the patient group in bilateral superior parietal lobes (BA 7, 40) and in the right prefrontal cortex, namely precentral (BA 4) and inferior frontal gyrus (BA 9) of the anticorrelated IC pattern of Fig. 1f/F.

Patients with aMCI Have Reduced Gray Matter Volume in the Medial Temporal Lobes. To assess possible causes of reduced functional connectivity, we analyzed our data for structural differences between both study groups. Neither the analyses of global volumes of gray matter (GM) and white matter (WM) nor the

[§§]Correa, N., Adali, T., Li, Y., and Calhoun, V. D. (2005) in Proceedings of the IEEE Conference on Acoustics, Speech, Signal Processing, Philadelphia, PA, pp. 401–404.

NEUROSCIENCE

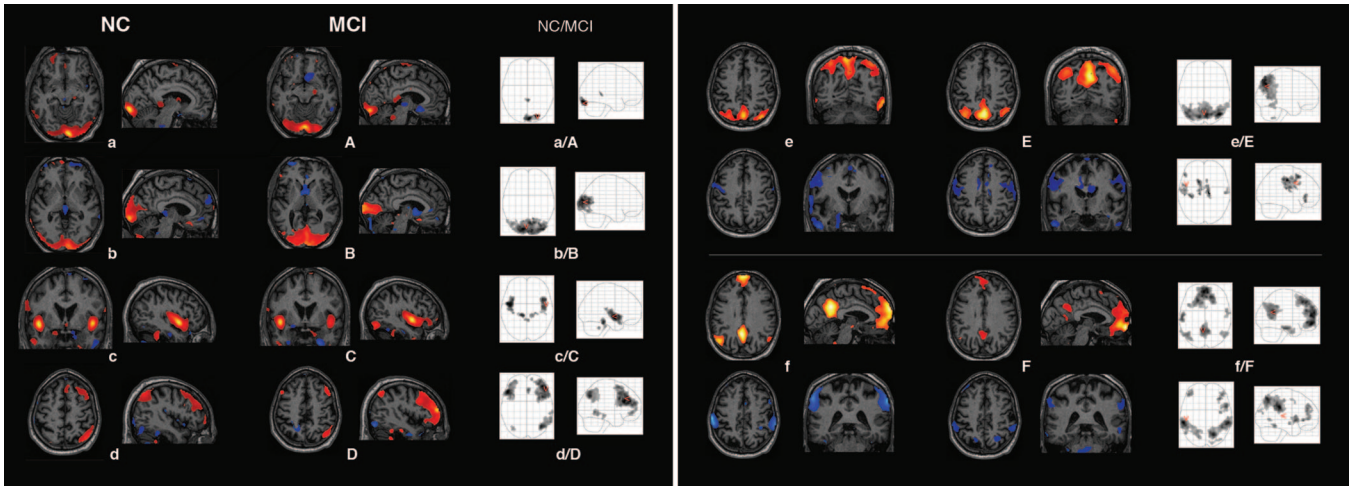

Fig. 1. RSNs of normal controls (*a*–f) and patients with aMCI (A–F). Each group IC image contains a pair of two spatial IC patterns that are correlated (red) or anticorrelated (blue) with the time course of the component (data not shown). (a/A–d/D) Each pair of IC patterns is shown within one brain image. (e/E and f/F) Each upper row represents the correlated IC pattern, each lower row the anticorrelated one. IC patterns are superimposed on a single-subject high-resolution T1 image. The black to yellow/light blue color scale represents *z* values, ranging from 1.8 to 8.0. Glass brain projections illustrate results of one-sample *t* tests on the individual back-reconstructed subject IC patterns across both groups ($P < 0.05$, FDR-corrected). (a/A–d/D) One-sample *t* test on the anticorrelated individual subject IC patterns provided no significant results. In axial view the right hemisphere is displayed on the right. NC, normal controls.

voxel-wise analysis of WM revealed significant differences. However, the voxel-wise analysis of GM revealed GM loss bilaterally in the MTL including the HC, the thalamus, the insular cortex, as well as in patches within the inferior parietal lobe (Fig. 3). These findings comply with previous reports on subtle abnormalities in structural brain images of patients with aMCI (16, 43). These areas did not overlap with those regions found to be altered in RSNs of the patient group.

At-Rest Coactivation of HC and PCC Is Absent in Patients with aMCI. To examine the relation of neocortical disconnectivity and MTL atrophy we investigated the functional connectivity between the HC and the RSNs with ROI correlation analyses. We hypothesized reduced coactivation of HC and PCC of the DMN in the patient group. The PCC is the central region of the posterior DMN that is primarily affected by AD-associated alterations such as hypometabolism or elevated atrophy rate; impaired PCC–MTL connectivity is assumed to be the main cause for prominent metabolic PCC changes in AD (3–7, 17). We computed the pairwise correlations between the time courses from each HC and the PCC cluster which was identified by ICA. The average correlation between left/right HC and PCC was $z = 0.37/0.30$, SE $= 0.08/0.08$ in the control group and $z = -0.03/-0.09$, SE $= 0.10/0.08$ in the patient group. We found significant group differences for each HC ($P = 0.04/0.02$, Bonferroni-

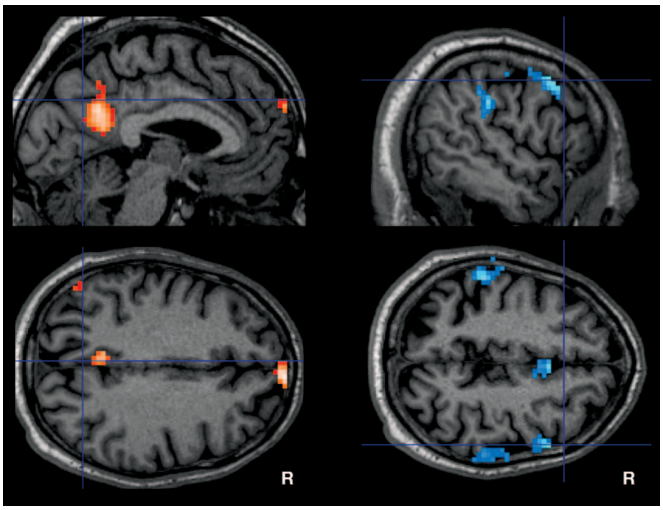

Fig. 2. Contrasts of RSNs between normal controls and patients with aMCI. (*Left*) Maps corresponding to DMNs of Fig. 1f/F, *Upper*. (*Right*) Maps corresponding to executive attention networks of Fig. 1f/F, *Lower*. Color maps represent significant ($P < 0.05$, FDR-corrected) voxels of higher component-related activity in controls compared with patients. Corresponding *t* values are color-coded with black to yellow (from 0 to 5.0) to light blue (from 0 to 6.2). Maps are superimposed on a single-subject high-resolution T1 image. The patient group did not show any significant higher activation for DMN and executive attention network. For all remaining RSNs of Fig. 1, two-sample *t* tests did not reveal any significant difference between the two groups. R, right hemisphere.

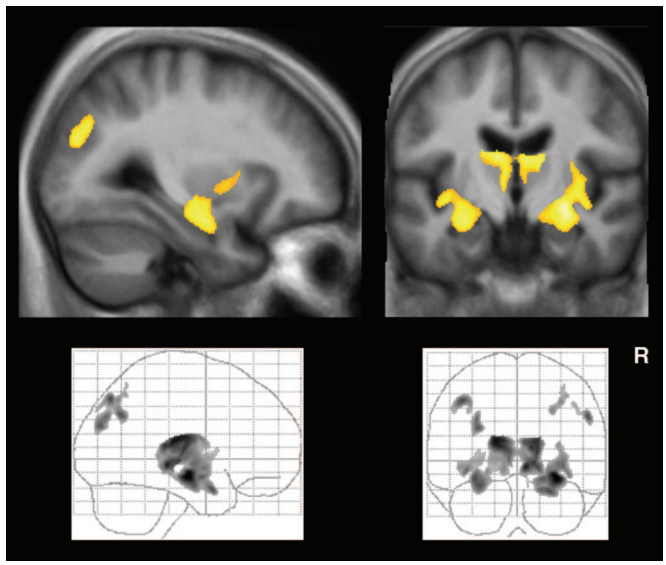

Fig. 3. Color maps showing significant ($P < 0.05$, FDR-corrected) voxels of decreased GM in aMCI compared with controls superimposed on sagittal and coronal slices transformed in standard MNI space. Corresponding *t* values are color-coded with black to yellow (from 0 to 6.3). The distribution of the complete regional pattern of decreased GM in patients is represented by glass brain projections.

corrected) by applying an analyses of covariance, which included corresponding HC volume as covariate. The correlation between left and right HC did not differ significantly between healthy controls ($z = 0.76$, SE = 0.10) and patients ($z = 0.62$, SE = 0.08) in a two-sample t test. To evaluate the degree of functional coactivation of the HCs and any RSN, we separately correlated the time courses of each HC with the time course of each RSN across all subjects. The strongest and only significant effect was found between left HC and the DMN ($z = 0.13$, SE = 0.06, $P = 0.003$, Bonferroni-corrected, one-sample t test), indicating relevant functional integration of the HC and the DMN during rest (5).

Discussion and Conclusion

In this work we investigated spatiotemporal patterns of hemodynamic activity during relaxed wakefulness and underlying brain volumes in healthy elderly and patients with amnestic MCI. By applying ICA, VBM, and ROI-based correlation analyses, we characterized eight RSNs that were spatially consistent across subjects and corresponded with functionally relevant patterns. Areas of the DMN and the executive attention network showed diminished functional connectivity in patients, whereas the respective volumes remained unaffected. Atrophy was found for both MTLs, including HCs in the patient group. Functional connectivity between both HCs and left PCC of the DMN was absent in patients. These results suggest that in aMCI a selected subset of RSNs is affected by altered functional connectivity, likely representing effects of early neurodegeneration.

Selectively Altered RSNs in Patients with aMCI. Our data suggest that disconnection phenomena associated with prodromal stages of AD are specific to a subset of RSNs whereas other networks remain unaffected. By applying ICA in patients with aMCI, we found left PCC and right medial prefrontal cortex of the DMN as well as bilateral superior parietal lobes and bilateral inferior frontal gyri of the executive attention network to be selectively affected (Fig. 2). Regions of the affected RSNs did not differ significantly in volumetric aspects between the two groups, confirming the functional nature of the observed alterations (Fig. 3). Our finding concerning the DMN is consistent with previous results demonstrating altered deactivation in regions of the DMN in MCI (44). The areas constituting the DMN and the executive attention network also seem to be involved in early changes of AD: In patients at risk for AD activity of the PCC or superior parietal cortex is changed during memory or executive attention-related tasks, respectively (14, 15). In mild AD, these regions show changed functional connectivity at rest (5, 9) and overlap with regional patterns of atrophy, glucose hypometabolism, and hypoperfusion (for overview, see ref. 3). Also, regions showing early amyloid deposition overlap with posterior parts of the default mode and executive attention network (2, 3, 45). In summary, our result of selective changes of RSNs in individuals at risk for AD corresponds very well with changes that have previously only been described in AD.

Changes of the MTL are discussed as a possible factor causing neocortical disconnectivity in AD (2, 4, 5, 7). The HC and posterior parts of the DMN display coherent spontaneous activity at rest (36) and constitute an episodic memory network that is linked to successful recollection (35). Functional connectivity of the HC with neocortical areas, especially with the PCC, is reduced in AD during rest (17). The VBM analysis (Fig. 3) demonstrated reduced GM within the MTL in the patient group. This finding is in line with previous results for aMCI (16, 43) and points to MTL neurodegeneration (3) as well as impaired MTL—neocortex connectivity (16). Our ROI correlation analysis revealed that both HCs show significantly reduced functional connectivity with the left PCC of the DMN in patients compared with controls. Among all RSNs, the DMN was functionally most strongly related to the HC at rest. This relation was demonstrated by the only significant correlation between left HC and DMN across all subjects, which is in line with previous results (5, 36). Taken together, the presented results indicate relevant functional integration of the HC in the DMN at rest as well as an impaired HC–parietal memory system in aMCI.

We conclude that the selectively changed functional connectivity of RSNs in individuals at high risk for AD reflects altered connectivity between the MTL and neocortical areas (4, 5, 7, 9, 15, 44). Apparently, MTL—neocortex disconnectivity is related to neurodegeneration, which is expressed by MTL atrophy (16). In addition to FC changes in the DMN, our result also points to relevant functional disconnectivity of the executive attention network, which is in line with observed attentional deficits in MCI and AD (9, 14, 15). This finding indicates impaired interaction between these two anticorrelated networks that prominently organize intrinsic brain activity (9, 22, 28). Finally, our work suggests that rest-fMRI has the potential for the evaluation of connectivity in patients at risk for AD for diagnostic purposes; one possible way would be to use ICA-derived patterns to define ROIs where FC analysis can classify patients from controls. We are currently in the process of assessing symptom progression in our patients in a two-year follow-up examination where FC analysis might provide a more accurate way to evaluate the risk of conversion to dementia for individual patients than neuropsychological testing and structural imaging alone.

RSNs and Functional Brain Disorders. In this work we identified spatially consistent RSNs across both study groups that match previous results (22, 24, 26, 46). Damoiseaux *et al.* (26) evaluated the spatial consistency of RSNs and found a set of 10 reliably detectable RSNs across subjects and sessions. Although we changed many parameters such as ICA model, age, and health condition of participants, the regional patterns of detected RSNs show large regional concordance with their findings. Identified RSNs can be divided into two groups. The spatial patterns of the first group (Fig. 1 a/A, b/B, c/C, and e/E) are associated with sensory or sensorimotor functions, characterized in several previous studies (23, 24, 46, 47). The remaining networks encompass regions involved in higher cognitive functions (34, 35, 41, 48, 49). The bilateral posterior parietal network of map *e/E* including precuneus and intraparietal sulcus is known to be associated with spatial attention processes (41). This network is anticorrelated to the RSN of map *e/E* representing regions normally involved in sensorimotor integration; areas of both networks are part of a functional system participating in goal-directed movement coordination (41). The spatial pattern of Fig. 1f/F (*Upper*) covers areas of the DMN; this network is suggested to support default mode function, such as maintaining a background level of attention for the detection of salient events by monitoring internal and external environment (49). Evidence increases that large parts of the posterior DMN together with the hippocampal system are associated with autobiographical and prospective memory processing (35, 36, 50). Both the network of Fig. 1f/F (*Lower*), involving bilateral superior parietal cortex, intraparietal sulcus, and inferior frontal gyrus, and the right lateralized frontoparietal network of Fig. 1d/D overlap with the regions of the dorsal/executive and ventral/reorienting attention systems (34). The dorsal attention system is assumed to be involved in top–down direction of attention, and the ventral system, lateralized to the right, supports reorienting of attention in response to salient stimuli (27). Rest fluctuations of the two systems, which are considered member of a group of areas routinely exhibiting task-related activation, are anticorrelated to spontaneous BOLD fluctuations of the DMN, demonstrated by ROI-based methods (22, 28). Using ICA, we found the anticorrelated coupling of the DMN limited to the dorsal attention network. Our result is supported by the finding that the two attention networks can be distinguished by their spontaneous rest activity (27); it seems plausible that a system concerned with attentional shifts in response to salient external

stimuli is less strongly connected to introspectively oriented default mode processing during rest than a system involved in goal-directed orienting of attention.

In summary, we identified eight distinct, partly anticorrelated, and spatially consistent RSNs in healthy elderly and patients with aMCI. The division of the rest-related BOLD signal into separate RSNs presumably reflects the functional organization of brain activity into stabilized functional–anatomical systems (18, 19, 31). Regarding the synchronicity of spontaneous BOLD fluctuations during rest, pathology-induced changes seem to exist also in patients with autism, schizophrenia, attention deficit hyperactivity disorder, or major depression (51–54). Taking into account these findings and our result of selective changes of RSNs in aMCI, we suggest that rest-fMRI and especially RSNs constitute very promising tools for the functional characterization of functional brain disorders, for intergroup comparisons, and possibly with some potential for assessing functional connectivity on a single-subject level.

Materials and Methods

Subject data and ICA of rest-fMRI data are described below. Detailed information regarding ROI-based correlation analyses of fMRI data and VBM analysis of structural MRI data can be found in *SI Materials and Methods*.

Subjects and Task. Sixteen healthy controls (6 female, ages 63–73 years) and 24 patients (11 female, ages 58–80 years) diagnosed with aMCI participated in the study. All subjects provided informed consent in accordance with the Human Research Committee guidelines of the Klinikum Rechts der Isar, Technische Universität, München. Patients were recruited from the Memory Clinic of the Department of Psychiatry, controls by word-of-mouth advertising. Examination of every subject included medical history, neurological examination, informant interview (only for patients), neuropsychological assessment [CERAD battery, Consortium to Establish a Registry for AD (55)], structural MRI, and for patients additional blood tests. Patients met criteria for aMCI which contain reported and neuropsychologically assessed memory impairments, largely intact activities of daily living, and excluded dementia (Table 1) (11). Exclusion criteria for entry into the study were other neurological, psychiatric, or systemic diseases (e.g., stroke, depression, alcoholism), or clinically remarkable MRI (e.g., stroke lesions) which could be related to cognitive impairment. Five controls and nine patients were treated for hypertension (β-blockers, angiotensin-converting enzyme inhibitors, and calcium channel blockers), and six controls and eight patients were treated for hypercholesterolemia (statins). None of the subjects had diabetes mellitus. None of the subjects or patients received psychotropic medication, especially cholinesterase inhibitors.

All subjects underwent 4 min of resting-state scan first followed by an attention and a memory task, which are not discussed here. For the resting-state scan, subjects were instructed simply to keep their eyes closed, not to think of anything in particular, and not to fall asleep.

Imaging Methods. Imaging was performed on a 1.5T Siemens Symphony system. Functional data were collected by using a gradient echo EPI sequence (TE = 50 ms, TR = 3,000 ms, flip angle = 90°, FoV = 200 mm^2, matrix = 64 × 64, 33 slices, slice thickness = 4 mm, and 0.4-mm interslice gap) (where TE is echo time, TR is repetition time, FoV is field of view, and T1 is inversion time) for a 4-min period resulting in a total of 80 volumes. The first three functional scans were discarded before the subsequent analysis. A T1-weighted anatomical dataset was obtained from each subject by using a magnetization-prepared rapid acquisition gradient echo sequence (TE = 3.93 ms, TR = 1,500 ms, TI = 760 ms, flip angle = 5°, FoV = 256 mm^2, matrix = 256 × 256, 160 slices, voxel size = 1 × 1 ×1 mm^3).

Preprocessing. Functional MRI data were preprocessed by using the Oxford Centre for Functional Magnetic Resonance Imaging of the Brain Software Library (FMRIB; FSL version 3.2), statistical parametric mapping (Wellcome Department of Cognitive Neurology; SPM5), and in-house software for Matlab (MathWorks).

In a first step, nonbrain structures were removed from the echo planar imaging volumes. Next we performed a mean-based intensity normalization of all slices within a volume by the same factor (56). Data were then motion-corrected, spatially normalized into the stereotactic space of the Montreal Neurological Institute (MNI), and spatially smoothed with an 8 × 8 × 8 mm Gaussian kernel with SPM5. Before they were entered into the ICA, a voxel-wise transformation was applied on the time course data $y_{ijk}(t), \hat{y}_{ijk}(t) = [y_{ijk}(t) - \langle y_{ijk} \rangle]/\sigma_{ijk}$ (for each voxel: t, time; i, j, k, three directions in space; $\langle y_{ijk} \rangle$, mean; σ_{ijk} standard deviation). This procedure removed any systematic, between-group differences with respect to BOLD amplitudes from the four-dimensional data set $\hat{y}_{ijk}(t)$. Sensitivity for variance correlation was thereby rendered independently of variance magnitude.

ICA. We performed the ICA by using group ICA for fMRI toolbox (GIFT version 1.3b; icatb.sourceforge.net)[§§] established for the analysis of fMRI data (15, 39, 54). The toolbox supports a group ICA approach, which first concatenates the individual data across time, followed by the computation of the subject-specific components and time courses. For each of the two study groups the toolbox performed the analysis in three stages: (*i*) data reduction, (*ii*) application of the ICA algorithm, and (*iii*) back-reconstruction for each individual subject (39).

In the first step (*i*), data from each subject were reduced by using PCA, whereby computational complexity was reduced and most of the information content of the data was preserved. After concatenating the resulting volumes, the number of independent sources was estimated by the GIFT dimensionality estimation tool based on the aggregated data: 28/31 ICs for the control/patient group (57). The final reduction step according to the selected number of components was achieved by PCA again. In the second stage of the analysis (*ii*) we chose the Infomax algorithm for running the proper IC analysis and a GM mask based on all subjects. In the final stage of back-reconstruction (*iii*), time courses and spatial maps were computed for each subject. After back-reconstruction, the mean spatial maps of each group were transformed to z scores for display (39). Before any statistics were applied to the individual subject maps, the initially calculated scaling factor σ_{ijk} was reintegrated into the data by voxel-wise multiplication.

Each IC contains a pair of two spatial IC patterns that are correlated or anticorrelated to the time course of the component. Upon visual inspection, eight IC patterns were located in the cortex and represented functionally relevant RSNs as described previously (26, 46). The remaining IC patterns were attributed to two major forms of artifacts: IC patterns representing tissue border artifacts near the ventricular system, the skull, and cerebrospinal fluid space or IC patterns with main activation in midbrain structures below $z = -20$ (MNI) in axial slices burdened by major vessel artifacts and lack of reliability in EPI scans. Individual subject IC patterns representing RSNs were entered into one- and two-sample random-effects analyses in SPM5. Results were thresholded at $P < 0.05$, FDR-corrected for multiple comparisons. The between-group two-sample t tests were masked with a within-group mask thresholded at $P < 0.05$, uncorrected.

We thank two reviewers for constructive suggestions. This work was supported by the German Federal Ministry of Education and Research Grant 01EV0710 and by Kommision für Klinische Forschung, Klinikum Rechts der Isar, München Grant 8765160.

1. Blennow K, de Leon MJ, Zetterberg H (2006) *Lancet* 368:387–403.
2. Braak H, Braak E (1991) *Acta Neuropathol* 82:239–259.
3. Buckner RL, Snyder AZ, Shannon BJ, LaRossa G, Sachs R, Fotenos AF, Sheline YI, Klunk WE, Mathis CA, Morris JC, *et al.* (2005) *J Neurosci* 25:7709–7717.
4. Meguro K, LeMestric C, Landeau B, Desgranges B, Eustache F, Baron JC (2001) *J Neurol Neurosurg Psychiatry* 71:315–321.
5. Greicius MD, Srivastava G, Reiss AL, Menon V (2004) *Proc Natl Acad Sci USA* 101:4637–4642.
6. Lavenex P, Suzuki WA, Amaral DG (2002) *J Comp Neurol* 447:394–420.
7. Blaizot X, Meguro K, Millien I, Baron JC, Chavoix C (2002) *J Neurosci* 22:9166–9170.
8. Van Hoesen GW (1997) *J Neuropsychiatry Clin Neurosci* 9:331–341.
9. Wang K, Liang M, Wang L, Tian L, Zhang X, Li K, Jiang T (2007) *Hum Brain Mapp* 28:967–978.
10. Delbeuck X, Van der Linden M, Collette F (2003) *Neuropsychol Rev* 13:79–92.
11. Gauthier S, Reisberg B, Zaudig M, Petersen RC, Ritchie K, Broich K, Belleville S, Brodaty H, Bennett D, Chertkow H, *et al.* (2006) *Lancet* 367:1262–1270.
12. Petersen RC, Smith GE, Waring SC, Ivnik RJ, Tangalos EG, Kokmen E (1999) *Arch Neurol* 56:303–308.
13. Dickerson BC, Salat DH, Greve DN, Chua EF, Rand-Giovannetti E, Rentz DM, Bertram L, Mullin K, Tanzi RE, Blacker D, *et al.* (2005) *Neurology* 65:404–411.
14. Dannhauser TM, Walker Z, Stevens T, Lee L, Seal M, Shergill SS (2005) *Brain* 128:1418–1427.
15. Celone KA, Calhoun VD, Dickerson BC, Atri A, Chua EF, Miller SL, DePeau K, Rentz DM, Selkoe DJ, Blacker D, *et al.* (2006) *J Neurosci* 26:10222–10231.
16. Stoub TR, DeToledo-Morrell L, Stebbins GT, Leurgans S, Bennett DA, Shah RC (2006) *Proc Natl Acad Sci USA* 103:10041–10045.
17. Wang L, Zang Y, He Y, Liang M, Zhang X, Tian L, Wu T, Jiang T, Li K (2006) *NeuroImage* 31:496–504.
18. Buckner RL, Vincent JL (2007) *NeuroImage* 37:1091–1096.
19. Fox MD, Raichle ME (2007) *Nat Rev Neurosci* 8:700–711.
20. Raichle ME, Mintun MA (2006) *Annu Rev Neurosci* 29:449–476.
21. Matthews PM, Honey GD, Bullmore ET (2006) *Nat Rev Neurosci* 7:732–744.
22. Fox MD, Snyder AZ, Vincent JL, Corbetta M, Van Essen DC, Raichle ME (2005) *Proc Natl Acad Sci USA* 102:9673–9678.
23. Hampson M, Peterson BS, Skudlarski P, Gatenby JC, Gore JC (2002) *Hum Brain Mapp* 15:247–262.
24. Biswal B, Yetkin FZ, Haughton VM, Hyde JS (1995) *Magn Reson Med* 34:537–541.
25. Beckmann CF, Smith SM (2004) *IEEE Trans Med Imaging* 23:137–152.
26. Damoiseaux JS, Rombouts SA, Barkhof F, Scheltens P, Stam CJ, Smith SM, Beckmann CF (2006) *Proc Natl Acad Sci USA* 103:13848–13853.
27. Fox MD, Corbetta M, Snyder AZ, Vincent JL, Raichle ME (2006) *Proc Natl Acad Sci USA* 103:10046–10051.
28. Fransson P (2005) *Hum Brain Mapp* 26:15–29.
29. Laufs H, Kleinschmidt A, Beyerle A, Eger E, Salek-Haddadi A, Preibisch C, Krakow K (2003) *NeuroImage* 19:1463–1476.
30. Mantini D, Perrucci MG, Del Gratta C, Romani GL, Corbetta M (2007) *Proc Natl Acad Sci USA* 104:13170–13175.
31. Vincent JL, Patel GH, Fox MD, Snyder AZ, Baker JT, Van Essen DC, Zempel JM, Snyder LH, Corbetta M, Raichle ME (2007) *Nature* 447:83–86.
32. Raichle ME, MacLeod AM, Snyder AZ, Powers WJ, Gusnard DA, Shulman GL (2001) *Proc Natl Acad Sci USA* 98:676–682.
33. Raichle ME, Snyder AZ (2007) *NeuroImage* 37:1083–1090.
34. Corbetta M, Shulman GL (2002) *Nat Rev Neurosci* 3:201–215.
35. Shannon BJ, Buckner RL (2004) *J Neurosci* 24:10084–10092.
36. Vincent JL, Snyder AZ, Fox MD, Shannon BJ, Andrews JR, Raichle ME, Buckner RL (2006) *J Neurophysiol* 96:3517–3531.
37. Buzsaki G, Draguhn A (2004) *Science* 304:1926–1929.
38. Calhoun VD, Adali T (2006) *IEEE Eng Med Biol Mag* 25:79–90.
39. Calhoun VD, Adali T, Pearlson GD, Pekar JJ (2001) *Hum Brain Mapp* 14:140–151.
40. Schmithorst VJ, Holland SK (2004) *J Magn Reson Imaging* 19:365–368.
41. Grefkes C, Fink GR (2005) *J Anat* 207:3–17.
42. De Luca M, Beckmann CF, De Stefano N, Matthews PM, Smith SM (2006) *NeuroImage* 29:1359–1367.
43. Whitwell JL, Petersen RC, Negash S, Weigand SD, Kantarci K, Ivnik RJ, Knopman DS, Boeve BF, Smith GE, Jack CR, Jr (2007) *Arch Neurol* 64:1130–1138.
44. Rombouts SA, Barkhof F, Goekoop R, Stam CJ, Scheltens P (2005) *Hum Brain Mapp* 26:231–239.
45. Klunk WE, Engler H, Nordberg A, Wang Y, Blomqvist G, Holt DP, Bergstrom M, Savitcheva I, Huang GF, Estrada S, *et al.* (2004) *Ann Neurol* 55:306–319.
46. Beckmann CF, Smith SM (2005) *NeuroImage* 25:294–311.
47. Xiong J, Parsons LM, Gao JH, Fox PT (1999) *Hum Brain Mapp* 8:151–156.
48. Alescio-Lautier B, Michel BF, Herrera C, Elahmadi A, Chambon C, Touzet C, Paban V (2007) *Neuropsychologia* 45:1948–1960.
49. Gusnard DA, Raichle ME, Raichle ME (2001) *Nat Rev Neurosci* 2:685–694.
50. Addis DR, Wong AT, Schacter DL (2007) *Neuropsychologia* 45:1363–1377.
51. Cherkassky VL, Kana RK, Keller TA, Just MA (2006) *NeuroReport* 17:1687–1690.
52. Greicius MD, Flores BH, Menon V, Glover GH, Solvason HB, Kenna H, Reiss AL, Schatzberg AF (2007) *Biol Psychiatry* 62:429–437.
53. Liang M, Zhou Y, Jiang T, Liu Z, Tian L, Liu H, Hao Y (2006) *NeuroReport* 17:209–213.
54. Garrity AG, Pearlson GD, McKiernan K, Lloyd D, Kiehl KA, Calhoun VD (2007) *Am J Psychiatry* 164:450–457.
55. Morris JC, Heyman A, Mohs RC, Hughes JP, van Belle G, Fillenbaum G, Mellits ED, Clark C (1989) *Neurology* 39:1159–1165.
56. Manjaly ZM, Marshall JC, Stephan KE, Gurd JM, Zilles K, Fink GR (2003) *NeuroImage* 19:674–683.
57. Li YO, Adali T, Calhoun VD (2007) *Hum Brain Mapp* 28:1251–1266.